

# Annals of Biomedical Engineering

## Evaluation of Cartilage Repair by Mesenchymal Stem Cells Seeded on a PEOT/PBT Scaffold in an Osteochondral Defect

--Manuscript Draft--

<b>Manuscript Number:</b>	ABME-D-14-00778
<b>Full Title:</b>	Evaluation of Cartilage Repair by Mesenchymal Stem Cells Seeded on a PEOT/PBT Scaffold in an Osteochondral Defect
<b>Article Type:</b>	Research Article
<b>Keywords:</b>	Additive manufacturing; 3D scaffold; PEOT/PBT; mesenchymal stem cells; cartilage repair.
<b>Corresponding Author:</b>	Mary Murphy IRELAND
<b>Corresponding Author Secondary Information:</b>	
<b>Corresponding Author's Institution:</b>	
<b>Corresponding Author's Secondary Institution:</b>	
<b>First Author:</b>	Valerie Barron, BSc PhD
<b>First Author Secondary Information:</b>	
<b>Order of Authors:</b>	Valerie Barron, BSc PhD Khalid Merghani Georgina Shaw Cynthia Coleman Jessica Hayes Sharon Ansboro Abi Manian Grace O'Malley Emma Connolly Anand Nandakumar Clemen van Blitterswijk Pamela Habibovic Lorenzo Moroni Fintan Shannon Frank Barry Mary Murphy
<b>Order of Authors Secondary Information:</b>	
<b>Abstract:</b>	The main objective of this study was to evaluate the effectiveness of a mesenchymal stem cell (MSC)-seeded polyethylene-oxide-terephthalate/polybutylene-terephthalate (PEOT/PBT) scaffold for cartilage tissue repair in an osteochondral defect using a rabbit model. Materials characterisation using scanning electron microscopy indicated that the scaffold had a 3D architecture characteristic of the rapid prototyping fabrication method, with a strut diameter of $296 \pm 52\mu\text{m}$ and a pore size of $512 \pm 22\mu\text{m} \times 476 \pm 25\mu\text{m} \times 180 \pm 30\mu\text{m}$ . Chemical and morphological properties were typical of the PEOT/PBT copolymer. Moreover, the scaffold did not evoke an adverse cell response

	<p>in vitro or an inflammatory response in vivo. In terms of histological evaluation, no statistical difference was observed between the cell-free and cell-seeded scaffolds. Seeding the PEOT/PBT scaffolds with MSCs appeared to produce better scores for surface continuity, tidemark, thickness of repair, integration with native cartilage and degenerative changes in de novo and native tissue compared to the contralateral knee implanted with cell-free scaffolds. In summary, MSCs in combination with a 3D PEOT/PBT scaffold created a reparative environment for cartilage repair.</p>
<p><b>Suggested Reviewers:</b></p>	<p>Kyriacos A. Athanasiou athanasiou@ucdavis.edu</p> <hr/> <p>Daniel Grande dgrande@nshs.edu</p> <hr/> <p>Brian Diekman bdiekman@email.unc.edu</p> <hr/> <p>Laura Creemers bdiekman@email.unc.edu</p>

**Evaluation of Cartilage Repair by Mesenchymal Stem Cells Seeded on a PEOT/PBT Scaffold in an Osteochondral Defect**

V. Barron<sup>1</sup>, K. Merghani<sup>1</sup>, G. Shaw<sup>1</sup>, C. M. Coleman<sup>1</sup>, JS. Hayes, S. Ansboro<sup>1</sup>, A. Manian<sup>1</sup>, G. O'Malley, E. Connolly<sup>1</sup>, A. Nandakumar<sup>3</sup>, C.A. van Blitterswijk<sup>3</sup>, P. Habibovic<sup>3</sup>, L. Moroni<sup>3</sup>, F. Shannon<sup>2</sup>, J.M. Murphy<sup>1\*</sup> and F. Barry<sup>1</sup>

<sup>1</sup>Regenerative Medicine Institute, National University of Ireland, Galway, Ireland.

<sup>2</sup>Discipline of Surgery, Clinical Science Institute, Galway University Hospital, National University of Ireland Galway, Ireland.

<sup>3</sup>Department of Tissue Regeneration, Institute for Biomedical Technology and Technical Medicine (MIRA), University of Twente, Enschede, The Netherlands.

\* Corresponding author

Email addresses: mary.murphy@nuigalway.ie

## Abstract

The main objective of this study was to evaluate the effectiveness of a mesenchymal stem cell (MSC)-seeded polyethylene-oxide-terephthalate/polybutylene-terephthalate (PEOT/PBT) scaffold for cartilage tissue repair in an osteochondral defect using a rabbit model. Materials characterisation using scanning electron microscopy indicated that the scaffold had a 3D architecture characteristic of the additive manufacturing fabrication method, with a strut diameter of  $296 \pm 52 \mu\text{m}$  and a pore size of  $512 \pm 22 \mu\text{m} \times 476 \pm 25 \mu\text{m} \times 180 \pm 30 \mu\text{m}$ . Chemical and morphological properties were typical of the PEOT/PBT copolymer. Moreover, the scaffold did not evoke an adverse cell response *in vitro* or an inflammatory response *in vivo*. In terms of histological evaluation, no statistical difference was observed between the cell-free and cell-seeded scaffolds. Seeding the PEOT/PBT scaffolds with MSCs appeared to produce better scores for surface continuity, tidemark, thickness of repair, integration with native cartilage and degenerative changes in *de novo* and native tissue compared to the contralateral knee implanted with cell-free scaffolds. In summary, MSCs in combination with a 3D PEOT/PBT scaffold created a reparative environment for cartilage repair.

**Key terms:** Additive manufacturing, 3D scaffold, PEOT/PBT, mesenchymal stem cells, cartilage repair

## 1. Introduction

Articular cartilage has a limited capacity for self-repair and tissue damage as a result of osteoarthritis or trauma generally has a poor outcome. Current surgical treatments for degenerative wear in the knee joint include microfracture, mosaicplasty, autologous chondrocyte implantation (ACI) or, more recently, matrix induced autologous chondrocyte implantation (MACI)<sup>2</sup>. Although in the shorter term these techniques improve mobility and alleviate pain, in many cases the repair tissue is fibrocartilaginous and lacks optimal biological and mechanical properties for long-term functional recovery<sup>12</sup>. Over the last 20 years, cell therapies and tissue engineering strategies have been investigated and have shown potential for the repair/regeneration of hyaline cartilage<sup>1</sup>. In particular, mesenchymal stem cells (MSCs) have shown promise as a suitable cell source as they can be harvested from bone marrow and other tissues and expanded in culture to obtain large numbers of cells with chondrogenic potential<sup>7</sup>.

Current matrix- or scaffold-associated strategies for cartilage tissue engineering rely on both non-degradable and biodegradable materials with structures optimized for cell seeding. There is now recognition that the mechanical properties, chemical composition, porosity and pore architecture of the scaffold play a very important role in cartilage repair, with recent studies focussing on creating bio-functional scaffolds with structures and properties similar to native cartilage<sup>21,22,29</sup>. Indeed, the authors developed a 3D, open pore polyethylene oxide terephthalate polybutylene terephthalate (PEOT/PBT) scaffold with a dynamic stiffness approaching that of native cartilage<sup>5,16,19,20</sup>. After 14 days of subcutaneous implantation, this construct appeared to be biocompatible and capable of supporting cartilaginous matrix deposition<sup>30</sup>. In an attempt to provide an integrated bioengineering solution to a current unmet biomedical problem, the main aim of this study was determine the effect of providing biological cues in addition to mechanical support on hyaline cartilage

1 repair after 12 weeks implantation in a rabbit model. To this end, porous PEOT/PBT  
2 scaffolds were fabricated by 3D-fiber deposition and the materials properties were evaluated  
3  
4 in terms of chemical composition, polymer morphology and mechanical properties. Upon  
5  
6 confirmation that the scaffolds did not evoke an adverse cell response when grown in the  
7  
8 presence of rabbit MSC, cell seeding was optimised using a fibronectin coating, while  
9  
10 biological cues for chondrogenesis were evaluated *in vitro* using a glycosaminoglycan  
11  
12 accumulation (GAG) assay. Thereafter, the cell-seeded scaffolds were implanted in an  
13  
14 osteochondral defect in a rabbit. After 12-weeks implantation, hyaline cartilage repair was  
15  
16 evaluated by histological staining, while blinded histological scoring was used to compare  
17  
18 examine the effect of providing biological cues from MSCs implanted on the PEOT/PBT  
19  
20 scaffold.  
21  
22  
23  
24  
25

## 26 **2. Materials and Methods**

### 27 **2.1 Materials**

28  
29  
30  
31 A 55/45-wt% PEOT/PBT scaffold created by 3D fibre deposition was employed in  
32  
33 this study. Scaffolds were produced at a melting temperature of 190°C, an extrusion pressure  
34  
35 of 4 bars, and an extrusion nozzle with an internal diameter of 0.7mm a 3D printer. A 0-90°  
36  
37 angle deposition pattern was followed in a layer-by-layer manner. The 3D architecture of the  
38  
39 scaffold was imaged using scanning electron microscopy (SEM) (Hitachi, S4700, UK). In  
40  
41 brief, samples were sputter coated with gold and imaged using a 15kV accelerating voltage  
42  
43 for analysis of strut diameter, pore width, height and depth. The chemical structure of the  
44  
45 scaffold was evaluated by Fourier transform infrared (FTIR) spectroscopy (FTIR-8300  
46  
47 Shimadzu, UK); spectra were recorded in the wavelength range of 4000 to 400cm<sup>-1</sup> by 2cm<sup>-1</sup>  
48  
49 resolution in 32 scans. Spectra were recorded in 10 different areas of each specimen (n=6).  
50  
51 The thermal properties of the scaffold were examined using differential scanning calorimetry  
52  
53 (DSC 60, Shimadzu, UK); 5mg of each sample was heated at a rate of 10°C/min from minus  
54  
55  
56  
57  
58  
59  
60  
61  
62  
63  
64  
65

1 50°C to 200°C, from which it was possible to determine the glass transition temperature ( $T_g$ )  
2 for both the PEOT and PBT regions of the copolymer and the crystalline melt temperature  
3  
4 ( $T_m$ ) of the PBT region (n=5). The percentage crystallinity ( $\chi\%$ ) was also determined for the  
5  
6 crystalline PBT region with a value of 144.5J/g for the heat of fusion ( $\Delta H_F$ ) for a pure PBT  
7  
8 crystal.<sup>4</sup> For both the *in vitro* and *in vivo* studies, the scaffolds were sterilized by immersion  
9  
10  
11 in 70% industrial methylated spirits (IMS) for 1 h.  
12  
13

## 14 **2.2 Cytotoxicity testing**

15  
16 Cytotoxicity test methods were employed to examine the cell response in the presence  
17  
18 of the PEOT/PBT scaffolds. Upon confirmation of rabbit MSC phenotype and surface marker  
19  
20 expression, MSCs were seeded at a density of 20,000 cells/cm<sup>2</sup> and maintained for 24h at  
21  
22 37°C in a humidified atmosphere of 5% CO<sub>2</sub> in cell culture medium consisting of alpha-  
23  
24 minimum essential medium ( $\alpha$ -MEM-Gibco) 10% fetal bovine serum (FBS) serum and 1%  
25  
26 penicillin/streptomycin (P/S) and 2% rabbit serum (RS). Thereafter, sectioned scaffolds, with  
27  
28 dimensions 1/10 of the total area of the well were placed directly on the cells and incubated  
29  
30 for an additional 24h. An AlamarBlue™ (AB) assay (Molecular Probes) was then employed  
31  
32 to examine the metabolic activity of the cells by measuring the fluorescence intensity (530nm  
33  
34 excitation/590 nm emission) on a microplate fluorescence reader (FLX800, Biotek  
35  
36 Instruments Inc.) as per the manufacturer's instruction. As a method of control, rabbit MSCs  
37  
38 seeded on tissue culture plastic were also examined (n=6).  
39  
40  
41  
42  
43  
44  
45

## 46 **2.3 Cell Seeding Optimisation**

47  
48 Previous studies have shown that a cell seeding density of 25 x 10<sup>6</sup> MSCs/ml is  
49  
50 required to achieve chondrogenesis in a 3D structure<sup>8</sup>. In addition, it has also been shown that  
51  
52 pre-coating the scaffolds with fibronectin enhances cell attachment<sup>13</sup>. As a consequence, four  
53  
54 concentrations of fibronectin 0, 25, 50 and 100  $\mu$ g/ml in PBS were evaluated as scaffold  
55  
56 coating materials. After 1h immersion in the fibronectin solutions, the PEOT/PBT scaffolds  
57  
58  
59  
60  
61  
62  
63  
64  
65

1 (3mm in diameter and 3mm in height) were placed in a 3ml EST Z sterile vacutainer (BD).  
2 Using a cell seeding density of  $25 \times 10^6$  cells/ml, a suspension of  $1.2 \times 10^6$  rabbit MSCs  
3 (passage 1) in 50 $\mu$ l of incomplete chondrogenic medium (ICM) consisting of HG-DMEM  
4 supplemented with 100nM dexamethasone, 50 $\mu$ g/ml ascorbic acid, 40 $\mu$ g/ml L-Proline,  
5 6.25 $\mu$ g/ml selenous acid, 5.33 $\mu$ g/ml linoleic acid, 1.25mg/ml bovine serum albumin,  
6 0.11mg/ml sodium pyruvate and 1% P/S containing was added to the vacutainer. Using an  
7 18-gauge needle and a 10ml syringe the air was aspirated from each tube by drawing a  
8 vacuum and releasing three times. The tubes containing the cell-seeded scaffolds were placed  
9 in an incubator at 37°C with 5% CO<sub>2</sub> for 1h to allow cell attachment and then immersed in  
10 1ml ICM to remove any unattached cells. Cell attachment was subsequently assessed by  
11 measurement of the total dsDNA content using a PicoGreen assay (Invitrogen). Cell  
12 distribution through the centre of the scaffold was assessed using SEM. Cell-seeded scaffolds  
13 were fixed in a 2.5% solution of electron microscopy grade gluteraldehyde, dehydrated in a  
14 series of alcohols from 50%-100% for 5 min each, dried by evaporation of  
15 hexamethyldisilazane, gold coated and imaged using SEM (Hitachi, UK) with an accelerating  
16 voltage of 15kV.

17  
18  
19  
20  
21  
22  
23  
24  
25  
26  
27  
28  
29  
30  
31  
32  
33  
34  
35  
36  
37  
38  
39 Previous studies have shown that MSC differentiation is enhanced in a hypoxic  
40 environment. The differentiation behavior of the rabbit MSC-seeded scaffold was evaluated  
41 by measuring GAG accumulation after 21 days culture in both hypoxic and normoxic  
42 environments. In brief, upon optimization of the fibronectin coating concentration, the rabbit  
43 MSC-seeded scaffolds were cultured in complete chondrogenic medium (CCM) consisting of  
44 ICM supplemented with 10ng/ml transforming growth factor (TGF)- $\beta$ 3) with medium  
45 changed every 2 days and cultured in either a hypoxic environment with 5% O<sub>2</sub> at 37°C and  
46 100% humidity or a normoxic environment with 21% O<sub>2</sub> at 37°C and 100% humidity.  
47  
48  
49  
50  
51  
52  
53  
54  
55  
56  
57  
58  
59  
60  
61  
62  
63  
64  
65  
Thereafter, GAG accumulation was determined using a dimethylmethylene (DMMB) assay

1 on papain digested scaffolds with chondroitin-sulphate-6 as a standard, while DNA was  
2 measured using a PicoGreen assay.  
3

#### 4 **2.4 Surgical Procedure**

5  
6  
7 Cartilage repair was assessed by implanting the cell-seeded scaffolds into a 3mm  
8  
9 osteochondral defect in the femoral condyle of a rabbit. Fifteen skeletally mature male white  
10  
11 New Zealand rabbits weighing at least 3kg were used according to University guidelines,  
12  
13 ethical approval from the Animal Care and Research Ethics Committee at the National  
14  
15 University of Ireland Galway and a licence from the Irish Department of Health. In brief, 30  
16  
17 knees were randomly assigned to 3 test groups, including empty defect (n=3 rabbits or 6  
18  
19 knees), cell free scaffold (n=6 rabbits or 12 knees) and cell-seeded scaffold (n=6 rabbits or 12  
20  
21 knees). Rabbits were anesthetized using a weight-adjusted dose of ketamine (35mg/kg) and  
22  
23 xylazine (10mg/kg) and a 3mm defect was created in the centre of the medial femoral  
24  
25 condyle using a drill with a previously sterilized 2.8mm drill bit covered with a sterile sheath.  
26  
27  
28 The walls of the defect were finished with a curette, and the PEOT/PBT scaffold was press-  
29  
30 fit into place. After 12 weeks, the rabbits were sacrificed and after examination of gross  
31  
32 surface morphology, the femoral condyles were removed and fixed in 10% neutral buffered  
33  
34 formalin and decalcified in Surgipath II for 2-3 weeks. Samples were serially sectioned at 5  
35  
36  $\mu\text{m}$  intervals and stained with toluidine blue. Immunohistochemistry was performed for  
37  
38 Collagen type I and Collagen type II as described previously<sup>23</sup> with minor modifications.  
39  
40 Sections were treated with 4 mg/ml (Dako Pepsin S3002) for 30 min at room temperature for  
41  
42 antigen retrieval prior to sequential incubation with a goat anti-type I collagen antibody  
43  
44 (1:100, S1310-01; SouthernBiotech) or a mouse anti-type II collagen antibody (1:50,  
45  
46 AF5710; Acris) at 4°C overnight followed by a biotinylated rabbit anti-goat secondary  
47  
48 (1:1000, 305-065-003; Jackson ImmunoResearch Inc.) for collagen type I and a goat anti-  
49  
50 mouse (1:1000; KPL 71-00-29) for collagen type II for 30 min at room temperature. Tissue  
51  
52  
53  
54  
55  
56  
57  
58  
59  
60  
61  
62  
63  
64  
65

1 sections were graded by four blinded reviewers, 1.5mm into the defect using the modified  
2 O'Driscoll scoring system based on previous studies<sup>10,28</sup>.  
3

## 4 **2.5 Statistical Analysis**

5  
6  
7 Where appropriate, results were represented as means  $\pm$  standard error of the mean  
8 (SEM). The histological scoring was analysed using Kruskal-Wallis (non-parametric)  
9 methods, with 95% confidence intervals used to examine statistical difference between the  
10 test subjects and ANOVA to examine statistical differences between the test groups. A p  
11 value of less than 0.05 was considered statistically significant (\*p < 0.05). All data was  
12 analysed using GraphPad Prism version 6.  
13  
14  
15  
16  
17  
18  
19  
20

## 21 **3. Results**

### 22 **3.1 Materials Characterisation of the 3D PEOT/PBT Scaffold**

23  
24  
25  
26  
27 As shown in Fig. 1A, SEM analysis demonstrated that the 3D PEOT/PBT scaffolds  
28 had a strut diameter of  $296 \pm 52 \mu\text{m}$  and a pore size of  $512 \pm 22 \mu\text{m} \times 476 \pm 25 \mu\text{m} \times 180 \pm$   
29  $30 \mu\text{m}$ . A typical FTIR spectrum for PEOT/PBT is observed in Fig. 1B, with characteristic  
30 peaks at  $1710\text{cm}^{-1}$  for the C=O group of the PBT region,  $1080\text{-}1180\text{cm}^{-1}$  for the C-O-C  
31 groups of the PBT region, and between  $870\text{-}940\text{cm}^{-1}$  for the CH<sub>3</sub> groups of both the PEO and  
32 PBT. In terms of thermal properties and polymer morphology, the PEOT region of the  
33 polymer is amorphous and exhibits a T<sub>g</sub> at minus 30 °C, while the PBT region of the polymer  
34 is semicrystalline, exhibits a T<sub>g</sub> of 17 °C, a T<sub>m</sub> at 147 °C, a  $\Delta H_m$  of 7.68 and a percentage  
35 crystallinity of 5.3% (Fig. 1C).  
36  
37  
38  
39  
40  
41  
42  
43  
44  
45  
46  
47

### 48 **3.2 Cell Viability in the Presence of the PEOT/PBT Scaffold**

49  
50  
51 Cytotoxicity of the 3D PEOT/PBT scaffold was assessed with an AlamarBlue™ assay  
52 showing that there was no statistical difference detected in the cell metabolic activity of  
53 rabbit MSCs grown on tissue culture plastic (TCP) or MSCs grown in the presence of the  
54 PEOT/PBT scaffolds (Fig. 2).  
55  
56  
57  
58  
59  
60  
61  
62  
63  
64  
65

### 3.3 Optimal Cell Seeding Conditions

The optimal cell attachment and distribution of rabbit MSCs on the PEOT/PBT scaffolds was determined using a cell seeding density of  $25 \times 10^6$  cells/ml. A statistically greater number of cells were retained on scaffolds pre-treated with 50  $\mu\text{g/ml}$  fibronectin, with over a 7-fold increase in cell retention over no coating, 3 times greater loading compared to the use of 25  $\mu\text{g/ml}$  and almost twice that of 100  $\mu\text{g/ml}$  fibronectin (Fig. 3A) with average values of 50,000, 210,000, 580,000 and 320,000 for 0, 25, 50 and 100 $\mu\text{g/ml}$  of fibronectin, respectively. This is further evidenced in the SEM images, where a greater number of cells were seen to attach to the scaffold with the 50  $\mu\text{g/ml}$  coating of fibronectin (Fig. 3B).

### 3.4 *In vitro* chondrogenesis

With respect to the differentiation behaviour of the rabbit MSC-seeded scaffolds *in vitro*, the provision of biological signals for chondrogenesis was confirmed as evidenced by the GAG accumulation observed in both hypoxic and normoxic environments (Fig.4). After 21 days culture in the presence of  $\text{TGF}\beta_3$ , 24 $\mu\text{g}/\mu\text{g}$  of GAG/DNA was measured for hypoxia cultured samples compared to 12 $\mu\text{g}/\mu\text{g}$  of GAG/DNA recorded for cell-seeded scaffolds cultured in normoxia.

### 3.5 Histological Evaluation of Repair

Fig. 5A shows representative images of toluidine blue stained sections of the complete rabbit condyle. 12 weeks after implantation, cartilage repair is observed in the empty defect, the defect containing the cell-free scaffold and cell-seeded scaffold. It can also be seen that PEOT/PBT scaffold has not completely degraded suggesting that mechanical support was provided throughout the 12 week period. Moreover, it appears that the presence of the cells provide a better environment for repair with fewer large defects observed in comparison to the cell-free scaffold. However, on closer examination at higher magnification in Fig. 5B, the quality of repair was not the same in all cases. As seen previously with rabbit

1 models, cartilage repair in empty defects was observed after 12 weeks, with 2 of the 6  
2 replicates (Fig. 5Av and 5Avi) showing a thin line of organized cartilage repair and surface  
3 continuity and 3 of the 6 showing a tidemark (Fig. 5Ai, 5Av and 5Avi). Moreover, 3  
4 replicates (Fig. 5Aii, 5Aiii and 5Aiv) also showed evidence of degenerative changes  
5 (moderate hypo or hypercellularity) in the adjacent tissue, chondrocyte clustering and  
6 degenerative changes in the repair tissue.  
7  
8  
9  
10  
11  
12  
13

14 With respect to the cell-free PEOT/PBT scaffolds, hyaline cartilage morphology was  
15 not observed in any of the defects; there was no evidence of a smooth articular surface and  
16 there was no tidemark present in the six replicates. The thickness of the repair tissue  
17 approached that of native tissue in 1 of 6 replicates and this was accompanied by partial  
18 integration with the native cartilage (Fig. 5Aix). However, there was some evidence of  
19 integration at one side of 2/6 replicates (Fig. 5Avii and 5Axii). There were no degenerative  
20 changes (slight to moderate hypo or hypercellularity) observed in the newly formed cartilage  
21 tissue, however, there were degenerative changes observed in the adjacent host cartilage in  
22 50% of replicates (Fig. 5Aviii, 5Ax and 5Axi). Regarding the cell-seeded scaffolds, a thin  
23 layer of cartilage was observed in 33% of the samples (Fig. 5Axiii, 5Axiv and 5Axvii). The  
24 thickness of the cartilage repair tissue and integration with native tissue was also improved,  
25 with half of the samples (Fig. 5Axiii, 5Axiv and 5Axvii) approaching thickness of native  
26 cartilage tissue and 33% of showing integration with native tissue (Fig. 5Axiii, 5Axiv and  
27 5Axvii).  
28  
29  
30  
31  
32  
33  
34  
35  
36  
37  
38  
39  
40  
41  
42  
43  
44  
45  
46  
47

48 In relation to chondrogenesis, there was evidence of GAG accumulation in and  
49 around the scaffolds struts of the cell-free scaffold (Fig. 5B). Chondrocyte cells were  
50 observed in their lacunae above the tidemark in both the cell-free (Fig. 5Bv-viii) and cell-  
51 seeded scaffolds (Fig. 5Bix-xii). Nonetheless there was evidence of hypocellularity in the  
52 cell-free scaffolds (Fig. 5Bvi-viii). In addition, chondrocyte clusters were observed in the  
53  
54  
55  
56  
57  
58  
59  
60  
61  
62  
63  
64  
65

1 cell-seeded constructs (Fig. 5Bx-xi) and the original cartilage at the margin of the defect in  
2 the empty defects (Fig. 5Biii-iv).  
3

4  
5 Repair tissue in cell-free scaffolds stained positive for type 1 collagen with intense  
6 staining throughout equivalent to that of adjacent normal bone indicating fibrous cartilage  
7 repair (Fig. 5Cv-vi). On the other hand staining in cell-loaded scaffolds was detected to a  
8  
9 much lesser extent with intensity almost equivalent to background in some areas (Fig. 5Cix-  
10  
11 x). Nonetheless, collagen type I was detected in the border zone and at the surface of the  
12  
13 repair tissue in the cell-seeded scaffolds (Fig. 5Cix) and the empty defect (Fig. 5Ci). With  
14  
15 respect to collagen type II (Fig. 5D), there was evidence of staining in the empty defect (Fig.  
16  
17 5Di-iv) and in both the cell-free (Fig. 5Dv-viii) and MSC-seeded scaffolds (Fig. 5Dix-xii).  
18  
19 As in the case of the collagen type I staining, the tideline was expanded in the cell-free (Fig.  
20  
21 5Dv) and cell-seeded scaffolds (Fig. 5Dix), with collagen type II staining observed above the  
22  
23 tideline in the cartilage zone. Visually, the cell-seeded scaffold appeared to have more  
24  
25 hyaline cartilage as evidenced by collagen type II and less fibrocartilage as evidenced by  
26  
27 collagen type I staining when compared to the cell-free scaffold.  
28  
29  
30  
31  
32  
33  
34  
35

36 With respect to bone repair, there was no difference observed between the structural  
37  
38 integrity of the bone in the defects containing cell-free scaffolds (Fig. 5Avii-xii) when  
39  
40 compared to cell-seeded scaffolds (Fig. 5Axiix-xviii). However, in terms of bone structure,  
41  
42 the cell-seeded scaffold promoted better repair. Additionally, no bone cysts were observed  
43  
44 for either the cell-free or cell-seeded scaffolds; however cysts were observed in the empty  
45  
46 defects (Fig. 5Aii, iv).  
47  
48  
49

### 50 ***3.5 Histological Scoring of Repair Tissue***

51 The observations described above for the histological evaluation (Fig. 5) echoed the  
52  
53 trends observed for the scores generated for the repair tissue shown in Table 2 and Fig. 6. In  
54  
55 terms of hyaline cartilage, articular surface continuity and tidemark, the cell-free scaffold  
56  
57  
58  
59  
60  
61  
62  
63  
64  
65

1 produced the lowest mean score of 0 in all categories compared to 1.17, 0.5, and 0.5,  
2 respectively, for the cell-seeded scaffold (Table 2 and Fig. 6A). The mean score for the  
3 thickness of the repair tissue was 7.9 times greater in the cell-seeded scaffold (1.33)  
4 compared to the empty scaffold (0.17), while the integration was almost 3 times greater with  
5 mean scores of 0.17 observed for the empty scaffold and values of 1 observed for the cell-  
6 seeded construct (Table 2 and Fig. 6B). There was no statistically significant difference  
7 observed between the test groups for repair and regeneration (Table 2), with *p*-values  
8 determined for percentage hyaline cartilage ( $p=0.59$ ), articular surface continuity ( $p=0.30$ ),  
9 tidemark ( $p=0.07$ ) and thickness of repair tissue (0.18). The empty defect appeared to  
10 promote a better repair for hyaline cartilage repair, articular surface continuity, tidemark,  
11 however, the cell-seeded scaffold gave the best score for thickness of repair.  
12  
13  
14  
15  
16  
17  
18  
19  
20  
21  
22  
23  
24  
25  
26

27 A similar trend was observed for integration and degenerative changes (Fig. 6B). In  
28 terms of degenerative changes in the repair tissue, the cell-seeded scaffold had a score of 0.63  
29 compared to 0 for the cell-free scaffold. Degenerative changes in adjacent tissue had mean  
30 scores of 0.71 and 0.67 respectively for the cell-free and cell-seeded scaffolds. Again, no  
31 statistical differences were observed between test groups with *p*-values greater than 0.05  
32 determined for integration ( $p=0.37$ ), degenerative changes in repair tissue ( $p=0.17$ ),  
33 degenerative changes in adjacent tissue ( $p=0.38$ ) and chondrocyte clustering ( $p=0.30$ ).  
34 Differences were observed within the test groups, suggesting variability in the rabbit  
35 population; however, the general trend revealed that there was better repair in the cell-seeded  
36 scaffold. Although, the empty defect has high scores, the scaffold material is still present in  
37 the cell-free and cell-seeded test groups, which may account for the lower scores for articular  
38 surface continuity and tidemark. However, the cell-seeded scaffold has comparable scores to  
39 the empty defect for thickness of repair tissue and integration, suggesting that the material,  
40 although not completely degraded after the 12-week period, may provide a better template  
41  
42  
43  
44  
45  
46  
47  
48  
49  
50  
51  
52  
53  
54  
55  
56  
57  
58  
59  
60  
61  
62  
63  
64  
65

1 and mechanical support for hyaline cartilage repair and tidemark formation as it degrades  
2 further over time. Taken together with the higher magnification images in Fig. 5B and  
3 collagen type I staining (Figure 5C), the tidemark, cellularity and repair tissue the PEOT/PBT  
4 scaffold appears to have repair potential in the presence of the MSCs.  
5  
6  
7  
8

#### 9 **4. Discussion**

10 In this study, PEOT/PBT scaffolds were created using the clinically scalable and  
11 reproducible rapid prototyping method of 3D fibre deposition. The 3D architecture of the  
12 scaffold and values measured for the strut diameter ( $296 \pm 52 \mu\text{m}$ ) and pore size ( $512 \pm 22$   
13  $\mu\text{m} \times 476 \pm 25 \mu\text{m} \times 180 \pm 30 \mu\text{m}$ ) were in accordance with design parameters and are  
14 comparable with structures previously used for cartilage repair<sup>5,20,30</sup>. In terms of chemical  
15 properties, the scaffold displayed the characteristic peaks for PEOT/PBT and corresponded  
16 well with previous studies by Radder<sup>24</sup>. The thermal analysis data also corresponds with  
17 previous studies;<sup>4</sup> in particular, the hydrophilic PEO phase, which imparts the elastic  
18 properties of copolymer, has a Tg of minus 30 °C, and the hydrophobic PBT phase, which  
19 provides the strength component has a Tg of 17 °C, a Tm of 147 °C and a percentage  
20 crystallinity of 5.3%.  
21  
22  
23  
24  
25  
26  
27  
28  
29  
30  
31  
32  
33  
34  
35  
36  
37  
38

39 Cell attachment on biomaterials coated with the extracellular matrix protein  
40 fibronectin has been shown to interact through the RGD (arg-gly-asp) ligand within  
41 fibronectin and integrins such as  $\alpha_5\beta_1$  and  $\alpha_5\beta_3$ <sup>17,25</sup>. It has also been shown that cell  
42 adhesion is mediated by the confirmation and spatial distribution of RGD ligands<sup>15</sup>.  
43 Moreover, it has been shown that there is an optimal RGD density for cell attachment<sup>17,26</sup>. In  
44 this study, fibronectin coating of the scaffold at 50  $\mu\text{g}/\text{ml}$  in combination with a cell seeding  
45 density of  $25 \times 10^6$  cells/ml or  $1.2 \times 10^6$  cells/scaffold, as selected previously<sup>8</sup>, resulted in  
46 optimal cell loading. Above 50  $\mu\text{g}/\text{ml}$  fibronectin, a decrease in cell attachment and a change  
47 in cell morphology was observed. This correlates with the findings of Massia and Hubbell<sup>17</sup>,  
48  
49  
50  
51  
52  
53  
54  
55  
56  
57  
58  
59  
60  
61  
62  
63  
64  
65

1 where a decrease in cell attachment and a change in morphology was shown above a  
2 threshold value in RDG ligand density and associated fibronectin concentration. Furthermore,  
3  
4 the MSCs were seen to be attached to the scaffold struts and distributed throughout the 3D  
5  
6 construct as proposed by Jansen for optimal cartilage repair<sup>6</sup>. With respect to the MSC  
7  
8 differentiation behaviour *in vitro*, GAG accumulation after 21 days culture in the presence  
9  
10 of TGF $\beta$ <sub>3</sub> in both normoxic and hypoxic conditions compared well to other studies<sup>3,18</sup>, with  
11  
12 GAG/DNA values in hypoxia twice that observed in normoxia.  
13  
14  
15

16  
17 To determine whether the addition of MSCs to the scaffold would enhance the  
18  
19 efficacy of the previously described scaffold<sup>5,6</sup>, rabbit MSCs were seeded in the scaffold and  
20  
21 implanted in a rabbit osteochondral defect. Upon evaluation of the gross morphology of the  
22  
23 joint after 12 weeks, the cell-seeded scaffold was observed to promote the generation of  
24  
25 cartilage-like tissue fill, in addition to evidence of zonal organisation of cells, a continuous  
26  
27 articular surface, a tidemark, scaffold integration with adjacent tissue, and reduced  
28  
29 degenerative changes in the repair tissue.  
30  
31  
32

33  
34 After 12 weeks implantation, histological evaluation of the scaffolds revealed that  
35  
36 both the cell free and cell-seeded scaffolds integrated well with the native tissue and stained  
37  
38 positive for GAG and collagen type II or hyaline cartilage. In terms of the hyaline cartilage  
39  
40 morphology, 50% of the implanted cell-seeded scaffolds appeared to have zonal organisation  
41  
42 of cells and a tidemark visible (Fig. 5B xiii, xiv, xvii) compared to the cell free scaffolds (Fig.  
43  
44 5B vii-xii). In most cases, the cells in the cell-seeded scaffolds appeared to form lacunae and  
45  
46 displayed a longitudinal arrangement, despite the presence of clusters. In contrast,  
47  
48 hypocellularity was observed in the cell-free scaffolds and there was no obvious cell  
49  
50 orientation. Regarding fibrocartilage development, positive collagen type I staining was not  
51  
52 observed to the same extent in the cell-seeded scaffold, suggesting fibrocartilage formation in  
53  
54  
55  
56  
57  
58  
59  
60  
61  
62  
63  
64  
65

1 the cell-free scaffold and hyaline-like cartilage formation in the cell-seeded scaffold, echoing  
2 the observations of Maehara<sup>14</sup>  
3

4  
5 Nonetheless, analysis with a modified O'Driscoll scoring system, revealed that there  
6  
7 was no statistical difference observed between the cell-free scaffold and the cell-seeded  
8  
9 scaffold (Table 2), with *p*-values greater than 0.05 determined for percentage hyaline  
10  
11 cartilage, articular surface continuity, tidemark, thickness of repair tissue, integration,  
12  
13 degenerative changes and chondrocyte clustering. Nonetheless, seeding the PEOT/PBT  
14  
15 scaffolds with MSCs appears to produce higher mean scores for hyaline cartilage generation  
16  
17 (1.17 compared to 0), articular surface continuity (0.50 versus 0, tidemark integrity (0.50  
18  
19 versus 0), thickness of repair tissue (1.33 versus 0.17), integration with native tissue (1.0  
20  
21 versus 0.17) and degenerative changes in the repair tissue (0.63 versus 0), when compared to  
22  
23 the contralateral knee implanted with cell-free PEOT/PBT scaffolds. When compared to  
24  
25 other cartilage repair studies using a cell-free PEOT scaffold, these results compare well with  
26  
27 Jansen,<sup>6</sup> where cartilage repair was not observed frequently, while bone repair and integration  
28  
29 with native tissue was observed. In contrast, the cell-seeded PEOT/PBT scaffold in this study  
30  
31 appeared to augment cartilage repair in addition to bone repair, with higher O'Driscoll scores  
32  
33 for percentage hyaline cartilage, surface continuity, tidemark and thickness of repair tissue  
34  
35 compared to the cell-free scaffolds (Fig. 5A). Although the data were not statistically  
36  
37 significant, these results reflect those generated by Løken<sup>11</sup> and Liu<sup>10</sup> where a higher degree  
38  
39 of tissue filling and a trend for better quality repair was observed with the addition of MSCs.  
40  
41 Moreover, Løken also observed that there was no statistically significant difference in the  
42  
43 repair observed between cell-free and MSC-seeded hyaluronan scaffolds<sup>11</sup>. In terms of  
44  
45 materials degradation, the slower degradation of the PEOT/PBT scaffold agrees with other  
46  
47 studies<sup>9,27</sup>, in particular where cell-free and cell-seeded polycaprolactone scaffold have  
48  
49  
50  
51  
52  
53  
54  
55  
56  
57  
58  
59  
60  
61  
62  
63  
64  
65

1 shown to aid repair in osteochondral defects in rabbit models, without showing evidence of  
2 bone cysts or inflammation<sup>9</sup>.  
3

4  
5 In summary, a 3D biocompatible, bio-functional PEOT/PBT scaffold was fabricated,  
6  
7 physically characterised, combined successfully with rabbit MSCs and implanted in a rabbit  
8  
9 model *in vivo* to assess its efficacy in supporting cartilage repair. Despite the fact, that there  
10  
11 were no statistically significant differences observed in the O’Driscoll scores for tissue repair  
12  
13 and regeneration, the histological evaluation appeared to show that the addition of the MSCs  
14  
15 to the scaffolds promoted the formation of a hyaline cartilage cell morphology in 50% of the  
16  
17 implants. In addition, there was evidence of hyaline cartilage development in the cell-seeded  
18  
19 constructs, as evidenced by the presence of collagen type II staining and limited collagen type  
20  
21 I staining. Nonetheless, further studies are required to assess the potential of the MSC-seeded  
22  
23 scaffold structure to support long term remodelling of the hyaline cartilage and underlying  
24  
25 bone.  
26  
27  
28  
29  
30

### 31 32 33 34 **Acknowledgements**

35  
36 This work was supported by Science Foundation Ireland (SFI) Strategic Research Cluster  
37  
38 (SRC), Grant No. SFI: 09/SRC B1794, Wellcome Trust Biomedical Vacation Scholarships  
39  
40 grant number WTD004448, the European Union’s 7th Framework Programme under grant  
41  
42 agreement no. HEALTH-2007-B-223298 (PurStem)  
43  
44  
45

### 46 47 **References**

- 48  
49  
50 1. Anderson, J. A., D. Little, A. P. Toth, C. T. Moorman, B. S. Tucker, M. G. Ciccotti, and  
51  
52 F. Guilak. Stem Cell Therapies for Knee Cartilage Repair: The Current Status of  
53  
54 Preclinical and Clinical Studies. *Am. J. Sports Med.* ,  
55  
56  
57 2013.doi:10.1177/0363546513508744  
58  
59  
60  
61  
62  
63  
64  
65

- 1  
2  
3  
4  
5  
6  
7  
8  
9  
10  
11  
12  
13  
14  
15  
16  
17  
18  
19  
20  
21  
22  
23  
24  
25  
26  
27  
28  
29  
30  
31  
32  
33  
34  
35  
36  
37  
38  
39  
40  
41  
42  
43  
44  
45  
46  
47  
48  
49  
50  
51  
52  
53  
54  
55  
56  
57  
58  
59  
60  
61  
62  
63  
64  
65
2. Bhosale, A. M., and J. B. Richardson. Articular cartilage: structure, injuries and review of management. *Br. Med. Bull.* 87:77–95, 2008.
3. Christensen, B. B., C. B. Foldager, O. M. Hansen, A. A. Kristiansen, D. Q. S. Le, A. D. Nielsen, J. V. Nygaard, C. E. Bünger, and M. Lind. A novel nano-structured porous polycaprolactone scaffold improves hyaline cartilage repair in a rabbit model compared to a collagen type I/III scaffold: in vitro and in vivo studies. *Knee Surg. Sports Traumatol. Arthrosc. Off. J. ESSKA* 20:1192–1204, 2012.
4. Deschamps, A. A., D. W. Grijpma, and J. Feijen. Poly(ethylene oxide)/poly(butylene terephthalate) segmented block copolymers: the effect of copolymer composition on physical properties and degradation behavior. *Polymer* 42:9335–9345, 2001.
5. Emans, P. J., E. J. P. Jansen, D. van Iersel, T. J. M. Welting, T. B. F. Woodfield, S. K. Bulstra, J. Riesle, L. W. van Rhijn, and R. Kuijer. Tissue-engineered constructs: the effect of scaffold architecture in osteochondral repair. *J. Tissue Eng. Regen. Med.* , 2012.doi:10.1002/term.1477
6. Jansen, E. J. P., J. Pieper, M. J. J. Gijbels, N. A. Guldmond, J. Riesle, L. W. Van Rhijn, S. K. Bulstra, and R. Kuijer. PEOT/PBT based scaffolds with low mechanical properties improve cartilage repair tissue formation in osteochondral defects. *J. Biomed. Mater. Res. A* 89:444–452, 2009.
7. Johnson, K., S. Zhu, M. S. Tremblay, J. N. Payette, J. Wang, L. C. Bouchez, S. Meeusen, A. Althage, C. Y. Cho, X. Wu, and P. G. Schultz. A Stem Cell–Based Approach to Cartilage Repair. *Science* 336:717–721, 2012.
8. Kavalkovich, K. W., R. E. Boynton, J. M. Murphy, and F. Barry. Chondrogenic differentiation of human mesenchymal stem cells within an alginate layer culture system. *In Vitro Cell. Dev. Biol. Anim.* 38:457–466, 2002.

- 1  
2  
3  
4  
5  
6  
7  
8  
9  
10  
11  
12  
13  
14  
15  
16  
17  
18  
19  
20  
21  
22  
23  
24  
25  
26  
27  
28  
29  
30  
31  
32  
33  
34  
35  
36  
37  
38  
39  
40  
41  
42  
43  
44  
45  
46  
47  
48  
49  
50  
51  
52  
53  
54  
55  
56  
57  
58  
59  
60  
61  
62  
63  
64  
65  
9. Lee, C. H., J. L. Cook, A. Mendelson, E. K. Moioli, H. Yao, and J. J. Mao. Regeneration of the articular surface of the rabbit synovial joint by cell homing: a proof of concept study. *Lancet* 376:440–448, 2010.
10. Liu, Y., X. Z. Shu, and G. D. Prestwich. Osteochondral defect repair with autologous bone marrow-derived mesenchymal stem cells in an injectable, in situ, cross-linked synthetic extracellular matrix. *Tissue Eng.* 12:3405–3416, 2006.
11. Løken, S., R. B. Jakobsen, A. Arøen, S. Heir, A. Shahdadfar, J. E. Brinchmann, L. Engebretsen, and F. P. Reinholt. Bone marrow mesenchymal stem cells in a hyaluronan scaffold for treatment of an osteochondral defect in a rabbit model. *Knee Surg. Sports Traumatol. Arthrosc. Off. J. ESSKA* 16:896–903, 2008.
12. Longo, U. G., S. Petrillo, E. Franceschetti, A. Berton, N. Maffulli, and V. Denaro. Stem cells and gene therapy for cartilage repair. *Stem Cells Int.* 2012:168385, 2012.
13. Mackle, J. N., D. J.-P. Blond, E. Mooney, C. McDonnell, W. J. Blau, G. Shaw, F. P. Barry, J. M. Murphy, and V. Barron. In vitro characterization of an electroactive carbon-nanotube-based nanofiber scaffold for tissue engineering. *Macromol. Biosci.* 11:1272–1282, 2011.
14. Maehara, H., S. Sotome, T. Yoshii, I. Torigoe, Y. Kawasaki, Y. Sugata, M. Yuasa, M. Hirano, N. Mochizuki, M. Kikuchi, K. Shinomiya, and A. Okawa. Repair of large osteochondral defects in rabbits using porous hydroxyapatite/collagen (HAp/Col) and fibroblast growth factor-2 (FGF-2). *J. Orthop. Res. Off. Publ. Orthop. Res. Soc.* 28:677–686, 2010.
15. Maheshwari, G., G. Brown, D. A. Lauffenburger, A. Wells, and L. G. Griffith. Cell adhesion and motility depend on nanoscale RGD clustering. *J. Cell Sci.* 113:1677–1686, 2000.

16. Malda, J., T. B. F. Woodfield, F. van der Vloodt, C. Wilson, D. E. Martens, J. Tramper, C. A. van Blitterswijk, and J. Riesle. The effect of PEGT/PBT scaffold architecture on the composition of tissue engineered cartilage. *Biomaterials* 26:63–72, 2005.
17. Massia, S. P., and J. A. Hubbell. An RGD spacing of 440 nm is sufficient for integrin alpha V beta 3-mediated fibroblast spreading and 140 nm for focal contact and stress fiber formation. *J. Cell Biol.* 114:1089–1100, 1991.
18. Matsiko, A., T. J. Levingstone, F. J. O'Brien, and J. P. Gleeson. Addition of hyaluronic acid improves cellular infiltration and promotes early-stage chondrogenesis in a collagen-based scaffold for cartilage tissue engineering. *J. Mech. Behav. Biomed. Mater.* 11:41–52, 2012.
19. Moroni, L., G. Poort, F. Van Keulen, J. R. de Wijn, and C. A. van Blitterswijk. Dynamic mechanical properties of 3D fiber-deposited PEOT/PBT scaffolds: an experimental and numerical analysis. *J. Biomed. Mater. Res. A* 78:605–614, 2006.
20. Moroni, L., J. R. de Wijn, and C. A. van Blitterswijk. Three-dimensional fiber-deposited PEOT/PBT copolymer scaffolds for tissue engineering: influence of porosity, molecular network mesh size, and swelling in aqueous media on dynamic mechanical properties. *J. Biomed. Mater. Res. A* 75:957–965, 2005.
21. Moutos, F. T., B. T. Estes, and F. Guilak. Multifunctional hybrid three-dimensionally woven scaffolds for cartilage tissue engineering. *Macromol. Biosci.* 10:1355–1364, 2010.
22. Moutos, F. T., L. E. Freed, and F. Guilak. A biomimetic three-dimensional woven composite scaffold for functional tissue engineering of cartilage. *Nat. Mater.* 6:162–167, 2007.
23. Murphy, J. M., D. J. Fink, E. B. Hunziker, and F. P. Barry. Stem cell therapy in a caprine model of osteoarthritis. *Arthritis Rheum.* 48:3464–3474, 2003.

- 1  
2  
3  
4  
5  
6  
7  
8  
9  
10  
11  
12  
13  
14  
15  
16  
17  
18  
19  
20  
21  
22  
23  
24  
25  
26  
27  
28  
29  
30  
31  
32  
33  
34  
35  
36  
37  
38  
39  
40  
41  
42  
43  
44  
45  
46  
47  
48  
49  
50  
51  
52  
53  
54  
55  
56  
57  
58  
59  
60  
61  
62  
63  
64  
65
24. Radder, A. M., J. A. Loon, G. J. Puppels, and C. A. Blitterswijk. Degradation and calcification of a PEO/PBT copolymer series. *J. Mater. Sci. Mater. Med.* 6:510–517, 1995.
  25. Ruoslahti, E. RGD and other recognition sequences for integrins. *Annu. Rev. Cell Dev. Biol.* 12:697–715, 1996.
  26. Le Saux, G., A. Magenau, T. Böcking, K. Gaus, and J. J. Gooding. The Relative Importance of Topography and RGD Ligand Density for Endothelial Cell Adhesion. *PLoS ONE* 6:e21869, 2011.
  27. Shao, X., J. C. H. Goh, D. W. Hutmacher, E. H. Lee, and G. Zigang. Repair of large articular osteochondral defects using hybrid scaffolds and bone marrow-derived mesenchymal stem cells in a rabbit model. *Tissue Eng.* 12:1539–1551, 2006.
  28. Solchaga, L. A., J. U. Yoo, M. Lundberg, J. E. Dennis, B. A. Huibregtse, V. M. Goldberg, and A. I. Caplan. Hyaluronan-based polymers in the treatment of osteochondral defects. *J. Orthop. Res. Off. Publ. Orthop. Res. Soc.* 18:773–780, 2000.
  29. Valonen, P. K., F. T. Moutos, A. Kusanagi, M. G. Moretti, B. O. Diekman, J. F. Welter, A. I. Caplan, F. Guilak, and L. E. Freed. In vitro generation of mechanically functional cartilage grafts based on adult human stem cells and 3D-woven poly(epsilon-caprolactone) scaffolds. *Biomaterials* 31:2193–2200, 2010.
  30. Woodfield, T. B. F., J. Malda, J. de Wijn, F. Péters, J. Riesle, and C. A. van Blitterswijk. Design of porous scaffolds for cartilage tissue engineering using a three-dimensional fiber-deposition technique. *Biomaterials* 25:4149–4161, 2004.

**Table 1****Histological Scoring System used to Grade 12-week Cartilage Repair Specimens**

---

Percentage of Repair Tissue that is Hyaline (%HC)		
100 – 125%		6
80-100%		8
60-80%		6
40-60%		4
20-40%		2
0-20%		0
Articular Surface Continuity (SC)		
Continuous and smooth		2
Continuous but rough		1
Discontinuous		0
Tidemark (TM)		
Present		2
Incomplete (degenerative, vessel crossing)		1
Absent		0
Thickness of repair tissue compared to host cartilage (TH)		
121-150% of normal cartilage		1
81-120% of normal cartilage		2
51-80% of normal cartilage		1
0-50% of normal cartilage		0
Integration of cartilage (IC)		
Complete (integrated at both sides)		2
Partial		1
Poor (Not integrated at both sides)		0
Degenerative changes in Repair Tissue (DC)		
Hypocellularity		
Normal cellularity		2

1	Slight to moderate hypocellularity or hypercellularity	1
2	Severe hypocellularity or hypercellularity	0
3		
4	Degenerative changes in adjacent cartilage (AC)	
5		
6	Normal cellularity, no clusters, no fibrillations	3
7		
8	Normal cellularity, mild clusters, superficial fibrillations	2
9		
10	Mild or moderate changes in cellularity, moderate fibrillations	
11		
12	Severe changes in cellularity, severe fibrillations	0
13		
14	Chondrocyte clustering	
15		
16	No clusters	2
17		
18	<25% of the cells	1
19		
20	25-100% of the cells	0
21		
22		
23		
24		
25	<hr/>	
26		
27		
28		
29		
30		
31		
32		
33		
34		
35		
36		
37		
38		
39		
40		
41		
42		
43		
44		
45		
46		
47		
48		
49		
50		
51		
52		
53		
54		
55		
56		
57		
58		
59		
60		
61		
62		
63		
64		
65		

**Table 2** Statistical analyses of histological scoring

<i>Results of Histological Scoring</i>									
Group	Specimens (n)	<i>Repair and Regeneration</i>				<i>Integration and Degeneration</i>			
		Percentage hyaline cartilage	Articular surface continuity	Tidemark	Thickness	Integration	Degenerative changes in repair tissue	Degenerative changes in adjacent tissue	Chondrocyte clustering
<b>Empty Defect</b>									
<i>Mean score</i>	6	2.58	0.96	1.33	0.83	1.17	1.00	1.50	1.83
<i>SD</i>		4.01	1.19	0.82	0.98	0.98	1.10	1.23	0.41
<i>95% Confidence interval</i>		-1.62-6.79	-0.29-2.21	0.48-2.20	-0.20-1.87	0.14-2.20	-0.15-2.15	0.22-2.79	1.41-2.27
<b>PEOT/PBT</b>									
<i>Mean score</i>	6	0	0	0	0.17	0.17	0	0.71	1
<i>SD</i>		0	0	0	0.41	0.41	0	1.19	1.10
<i>95% Confidence interval</i>		0-0	0-0	0-0	-0.26-0.60	-0.26-0.60	0-0	-0.54-1.96	-0.15-2.15
<b>PEOT/PBT+ MSC</b>									
<i>Mean score</i>	6	1.17	0.50	0.50	1.33	1.00	0.63	0.67	0.83
<i>SD</i>		2.86	0.50	0.84	0.82	0.89	0.74	0.52	0.98
<i>95% Confidence interval</i>		-1.83-4.17	-0.08-1.08	-0.38-1.38	0.48-2.19	0.06-1.94	-0.15-1.40	0.13-1.21	-0.20-1.87
<b>Kruskal Wallis non-parametric test (ANOVA )</b>									
<i>p-value</i>		0.59	0.30	0.07	0.18	0.37	0.17	0.38	0.30

## Figure Legends

1  
2  
3 **FIG. 1.** Materials characterisation with (A) SEM images showing the 3D scaffold  
4 architecture from (i) top view and (ii) cross-section (B) FTIR spectrum for PEOT/PBT, with  
5 characteristic peaks at  $1710\text{ cm}^{-1}$  for the C=O group of the PBT region, between 1080-1180  
6  $\text{cm}^{-1}$  for the C-O-C groups of the PBT region, and between  $870\text{-}940\text{ cm}^{-1}$  for the  $\text{CH}_3$  groups  
7 of both the PEO and PBT regions. (C) DSC thermogram showing characteristic  $T_{gs}$  for PEOT  
8 (minus  $30^\circ\text{C}$ ) and PBT ( $17^\circ\text{C}$ ) and the crystalline melt temperature ( $T_m$ ) of the PBT region  
9 ( $147^\circ\text{C}$ ) of the polymer with inset highlighting the Tg region between  $-40^\circ\text{C}$  and  $40^\circ\text{C}$ . The  
10 percentage crystallinity was determined from the area under the curve at  $147^\circ\text{C}$ .  
11  
12  
13  
14  
15  
16  
17  
18  
19  
20  
21  
22  
23  
24  
25  
26

27 **FIG.2.** Viability of rabbit MSCs in the presence of the fabricated PEOT/PBT scaffold  
28 compared to controls on tissue culture plastic (TCP).  
29  
30  
31

32  
33  
34  
35 **FIG. 3.** (A) Cell seeding optimisation showing the greatest number of cells remaining on the  
36 scaffolds at 24 h. using  $50\mu\text{g/ml}$  fibronectin ( $n=3$ ). (B) Representative SEM images showing  
37 cell attachment on scaffolds coated with (i)  $0\mu\text{g/ml}$  fibronectin (ii)  $25\mu\text{g/ml}$  fibronectin, (iii)  
38  $50\mu\text{g/ml}$  fibronectin and (iv)  $100\mu\text{g/ml}$  fibronectin. Black arrows show cells on scaffold struts.  
39  
40  
41  
42  
43  
44  
45  
46  
47  
48  
49

50 **FIG.4.** *In vitro* chondrogenesis of MSCs loaded on PEOT/PBT scaffolds represented by  
51 GAG/DNA accumulation in hypoxic and normoxic cell culture environments. (Results are  
52 representative of assays performed for 1 donor with  $n=3$ ).  
53  
54  
55  
56  
57  
58  
59  
60  
61  
62  
63  
64  
65

1  
2  
3  
4  
5  
6  
7  
8  
9  
10  
11  
12  
13  
14  
15  
16  
17  
18  
19  
20  
21  
22  
23  
24  
25  
26  
27  
28  
29  
30  
31  
32  
33  
34  
35  
36  
37  
38  
39  
40  
41  
42  
43  
44  
45  
46  
47  
48  
49  
50  
51  
52  
53  
54  
55  
56  
57  
58  
59  
60  
61  
62  
63  
64  
65

**FIG. 5.** (A) Light microscopy images showing toluidine blue staining of cartilage repair (i-vi) in the empty defects, (vii-xii) the cell-free PEOT/PBT scaffolds and (xiii-xvii) the rabbit MSC-seeded scaffolds after 12 weeks implantation, magnification 1.25X. (B) Representative images showing toluidine blue staining for GAG accumulation in (i-iii) an empty defect, (iv-vi) a cell-free PEOT/PBT scaffold and (vii-ix) a rabbit MSC-seeded scaffold. (C) Immunohistological staining for collagen type I for (i-iii) a representative empty defect, (iv-vi) a cell-free PEOT/PBT scaffold and (vii-ix) a rabbit MSC-seeded scaffold. (D) Immunohistological staining for collagen type II counterstained with Harris haematoxylin for (i-iii) a representative empty defect, (iv-vi) a cell-free PEOT/PBT scaffold and (vii-ix) a rabbit MSC-seeded scaffold. Images show increasing magnification from left to right: 4x, 10x and 20x, respectively. Dotted lines highlight the repair tissue in the empty defects.

**FIG. 6.** Scores generated using a modified O’Driscoll scoring system for histological evaluation of (A) Tissue repair and regeneration (B) Integration and degeneration of repair tissue and adjacent tissue for empty defects, cell-free scaffolds and cell-seeded scaffolds. Dotted red lines indicate the highest possible score. (Results are representative of blinded evaluations performed by 4 evaluators. Values plotted are means  $\pm$  SEM).

1  
2  
3  
4  
5  
6  
7  
8  
9  
10  
11  
12  
13  
14  
15  
16  
17  
18  
19  
20  
21  
22  
23  
24  
25  
26  
27  
28  
29  
30  
31  
32  
33  
34  
35  
36  
37  
38  
39  
40  
41  
42  
43  
44  
45  
46  
47  
48  
49  
50  
51  
52  
53  
54  
55  
56  
57  
58  
59  
60  
61  
62  
63  
64  
65

Figure 1A 3D Architecture of scaffold

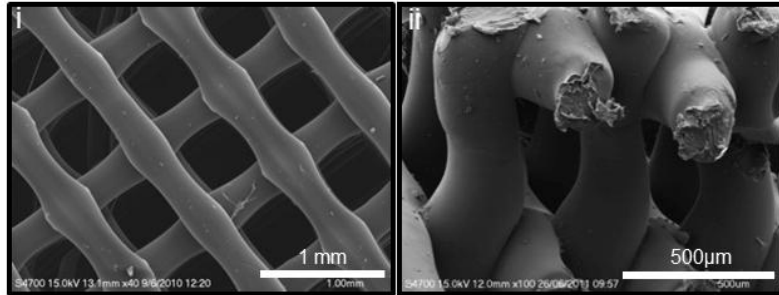


Figure 1B Chemical properties of scaffold

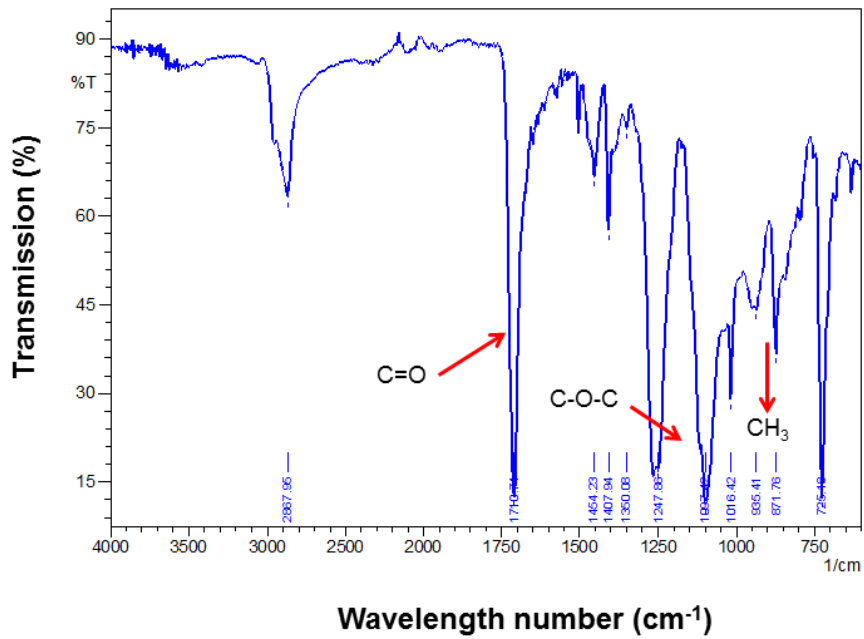


Figure 1C Thermal properties of scaffold

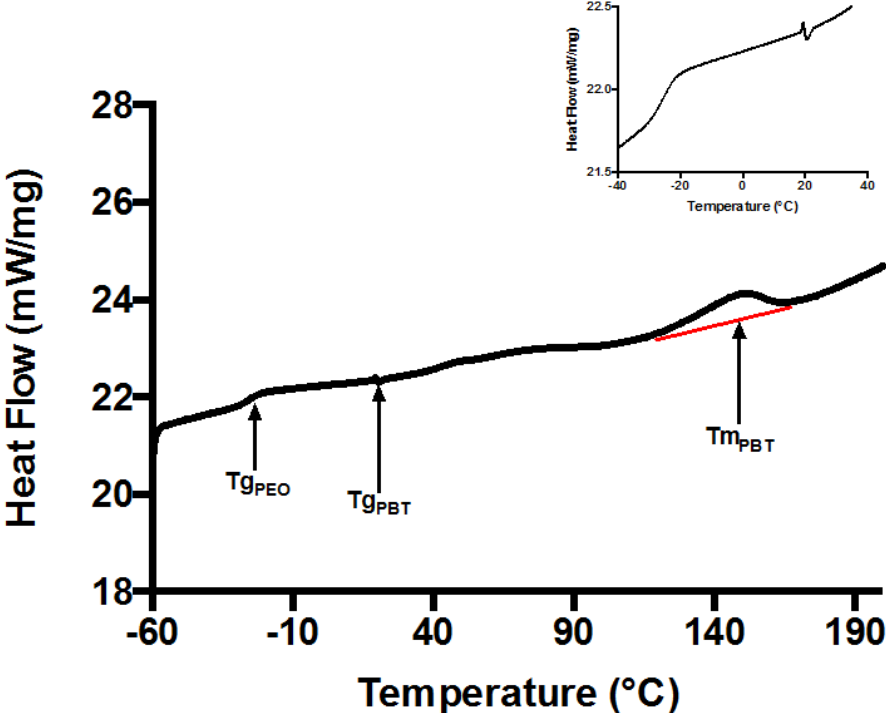
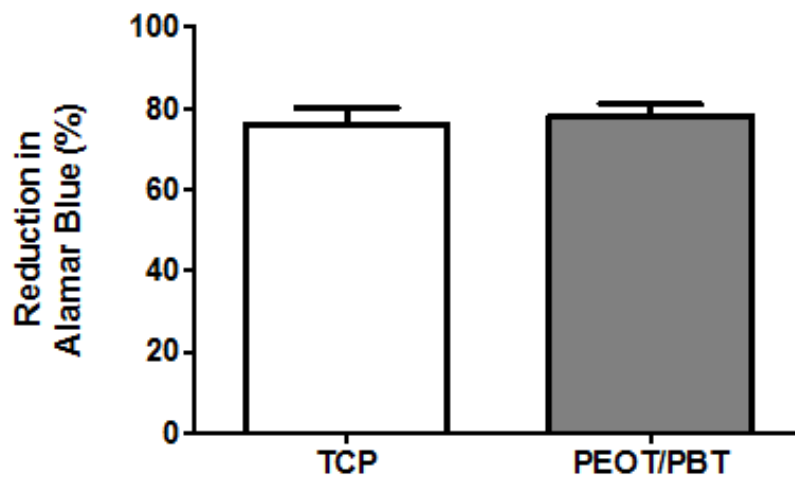


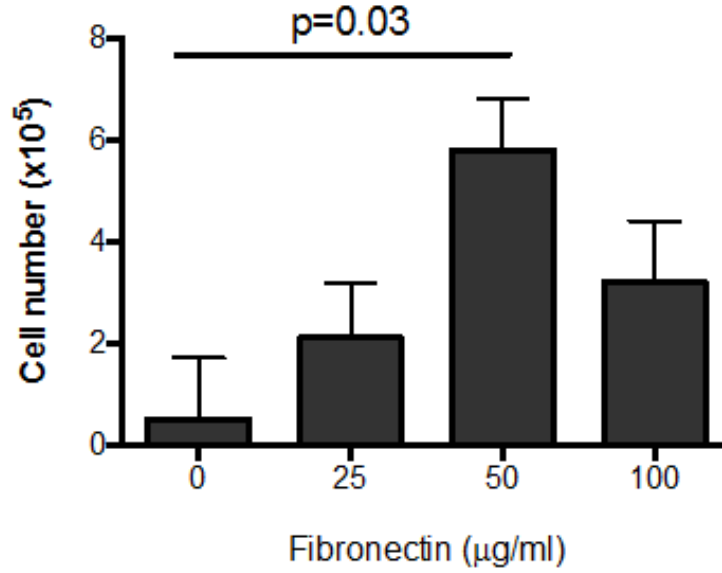
Figure 2 Cell metabolic activity in the presence of the PEOT/PBT scaffold.



1  
2  
3  
4  
5  
6  
7  
8  
9  
10  
11  
12  
13  
14  
15  
16  
17  
18  
19  
20  
21  
22  
23  
24  
25  
26  
27  
28  
29  
30  
31  
32  
33  
34  
35  
36  
37  
38  
39  
40  
41  
42  
43  
44  
45  
46  
47  
48  
49  
50  
51  
52  
53  
54  
55  
56  
57  
58  
59  
60  
61  
62  
63  
64  
65

Figure 3 Optimal fibronectin concentration for seeding the scaffold with MSCs

A



B

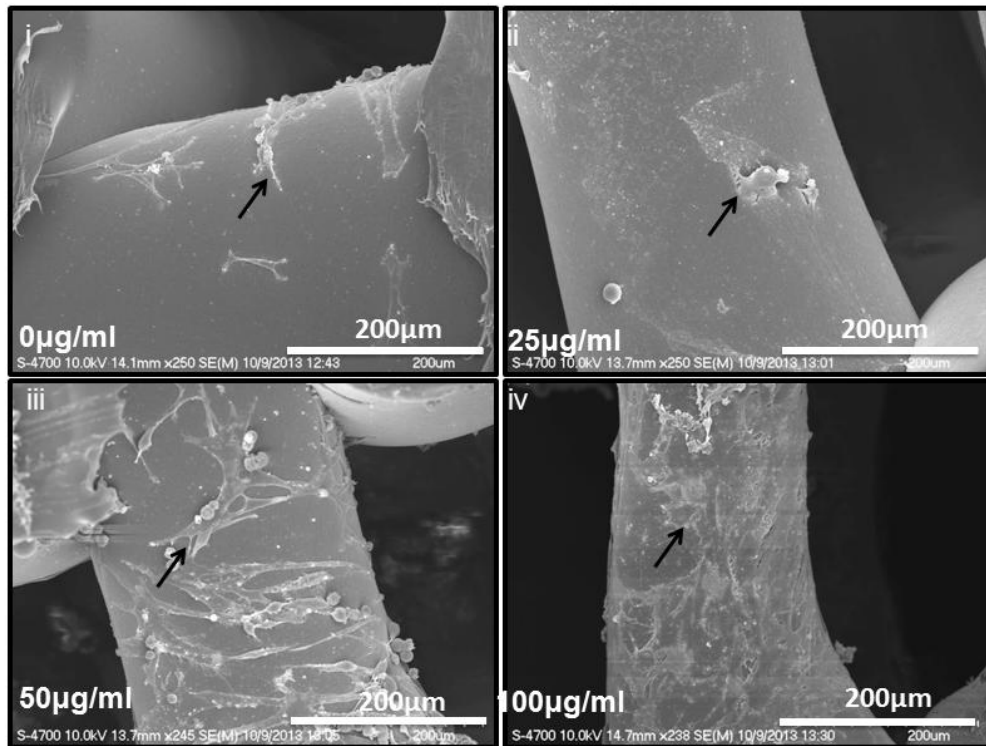
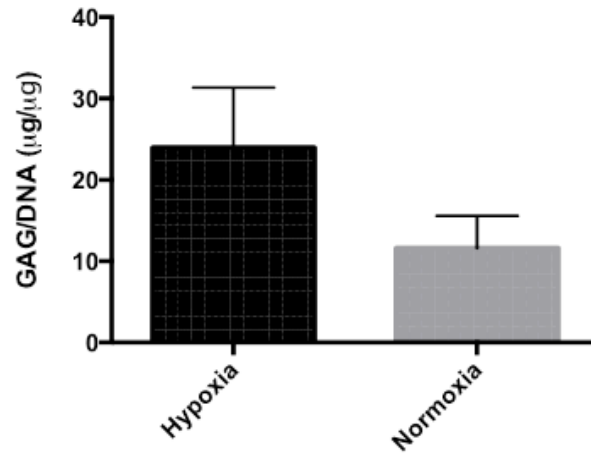


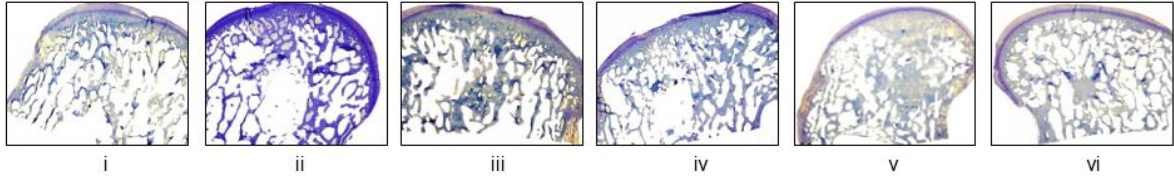
Figure 4 GAG accumulation is improved in hypoxic environment



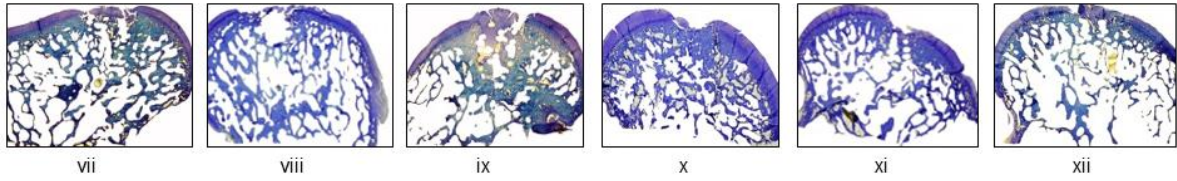
1  
2  
3  
4  
5  
6  
7  
8  
9  
10  
11  
12  
13  
14  
15  
16  
17  
18  
19  
20  
21  
22  
23  
24  
25  
26  
27  
28  
29  
30  
31  
32  
33  
34  
35  
36  
37  
38  
39  
40  
41  
42  
43  
44  
45  
46  
47  
48  
49  
50  
51  
52  
53  
54  
55  
56  
57  
58  
59  
60  
61  
62  
63  
64  
65

Figure 5A. Histological staining showing rabbit condyle

**Empty Defect**



**Cell-free PEOT/PBT Scaffold**



**Cell-seeded PEOT/PBT Scaffold**

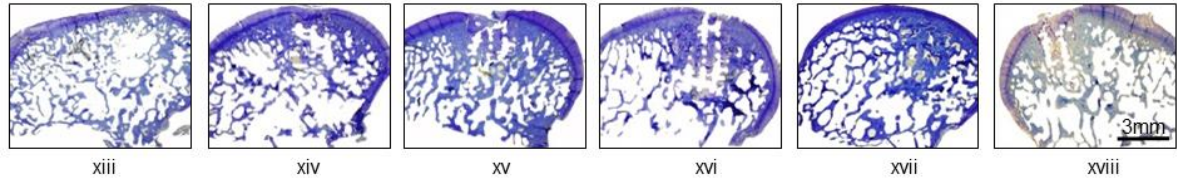
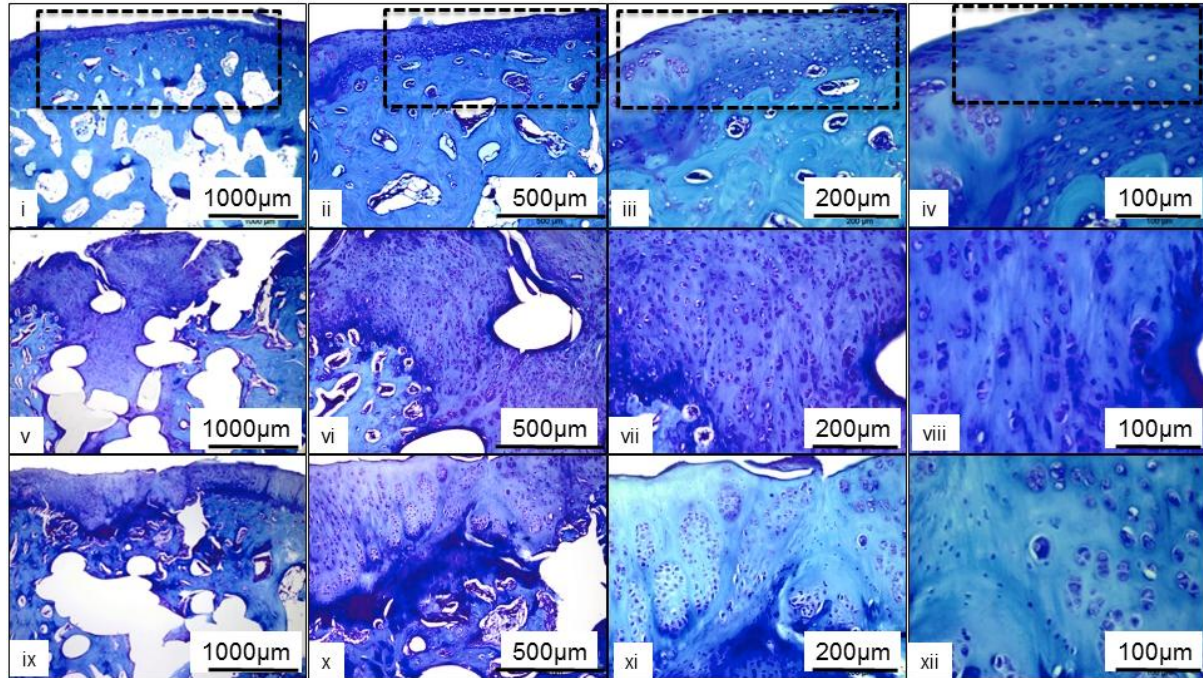


Figure 5B. Toluidine blue staining comparing GAG accumulation in empty defect, cell-free scaffold and cell-seeded scaffold



1  
2  
3  
4  
5  
6  
7  
8  
9  
10  
11  
12  
13  
14  
15  
16  
17  
18  
19  
20  
21  
22  
23  
24  
25  
26  
27  
28  
29  
30  
31  
32  
33  
34  
35  
36  
37  
38  
39  
40  
41  
42  
43  
44  
45  
46  
47  
48  
49  
50  
51  
52  
53  
54  
55  
56  
57  
58  
59  
60  
61  
62  
63  
64  
65

Figure 5C. Collagen type I staining comparing hyaline cartilage formation in empty defect, cell-free scaffold and cell-seeded scaffold

1  
2  
3  
4  
5  
6  
7  
8  
9  
10  
11  
12  
13  
14  
15  
16  
17  
18  
19  
20  
21  
22  
23  
24  
25  
26  
27  
28  
29  
30  
31  
32  
33  
34  
35  
36  
37  
38  
39  
40  
41  
42  
43  
44  
45  
46  
47  
48  
49  
50  
51  
52  
53  
54  
55  
56  
57  
58  
59  
60  
61  
62  
63  
64  
65

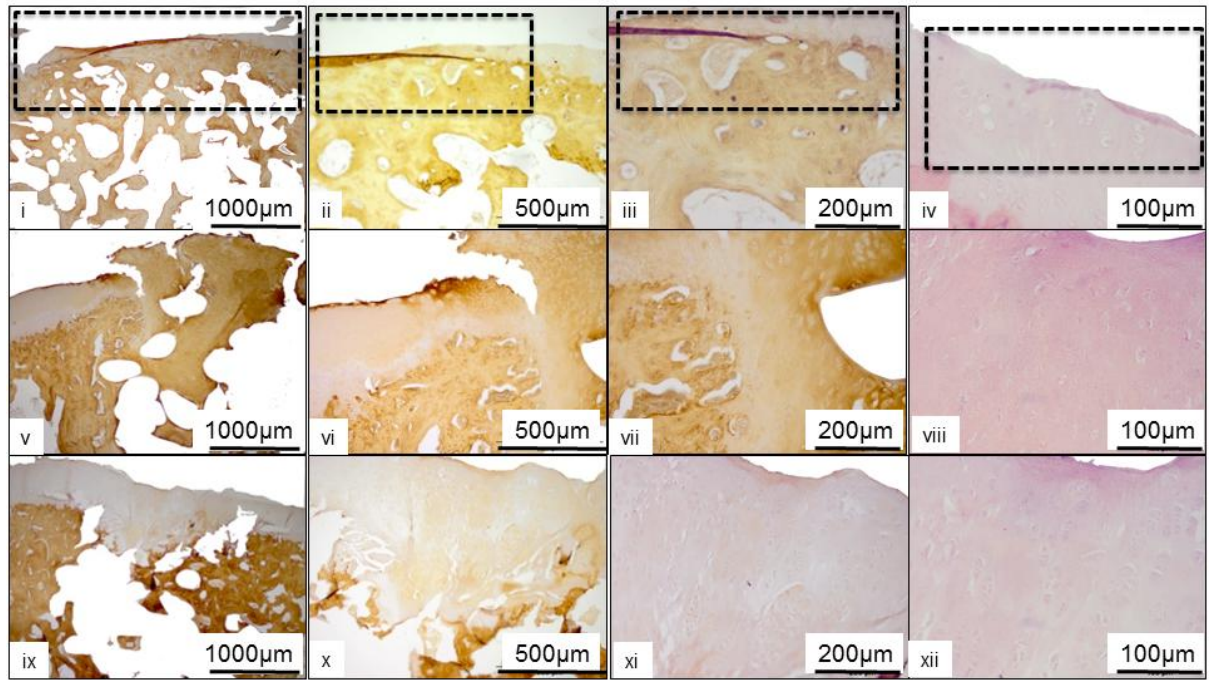


Figure 5D. Collagen type II staining comparing fibrocartilage formation in empty defect, cell-free scaffold and cell-seeded scaffold.

1  
2  
3  
4  
5  
6  
7  
8  
9  
10  
11  
12  
13  
14  
15  
16  
17  
18  
19  
20  
21  
22  
23  
24  
25  
26  
27  
28  
29  
30  
31  
32  
33  
34  
35  
36  
37  
38  
39  
40  
41  
42  
43  
44  
45  
46  
47  
48  
49  
50  
51  
52  
53  
54  
55  
56  
57  
58  
59  
60  
61  
62  
63  
64  
65

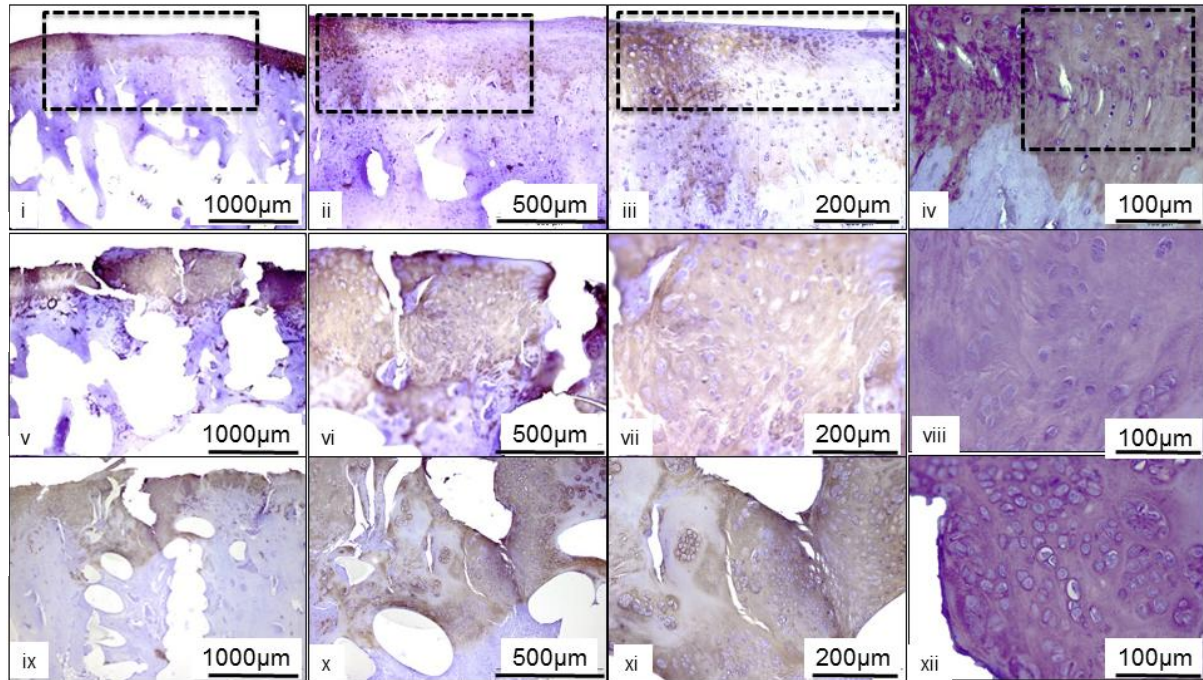
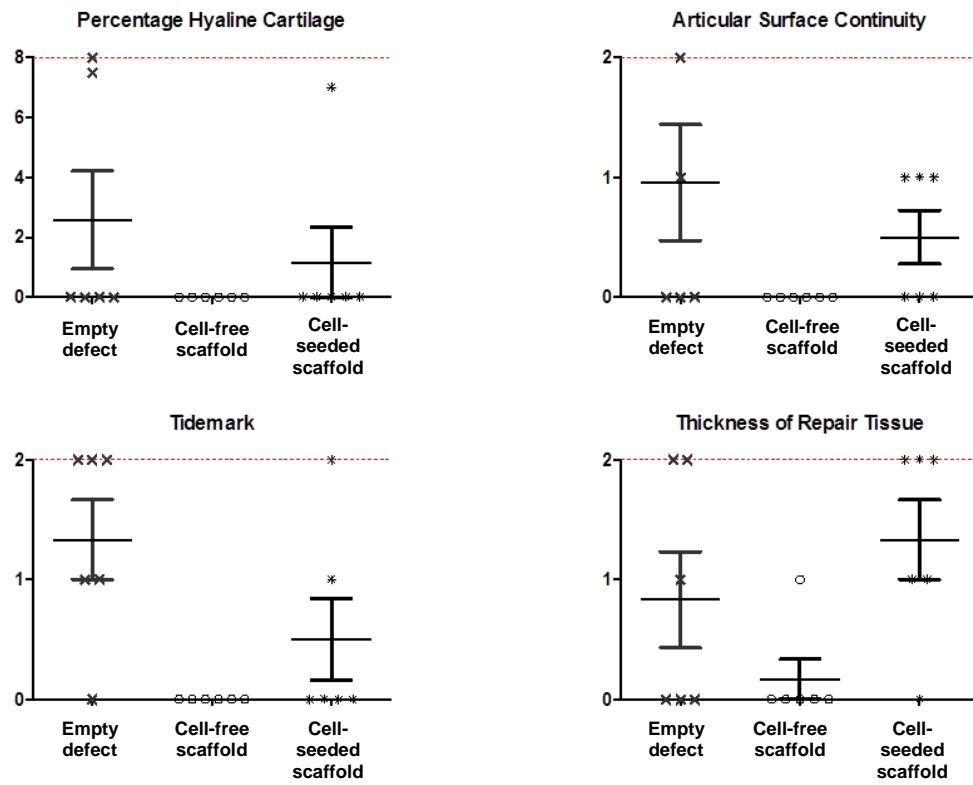
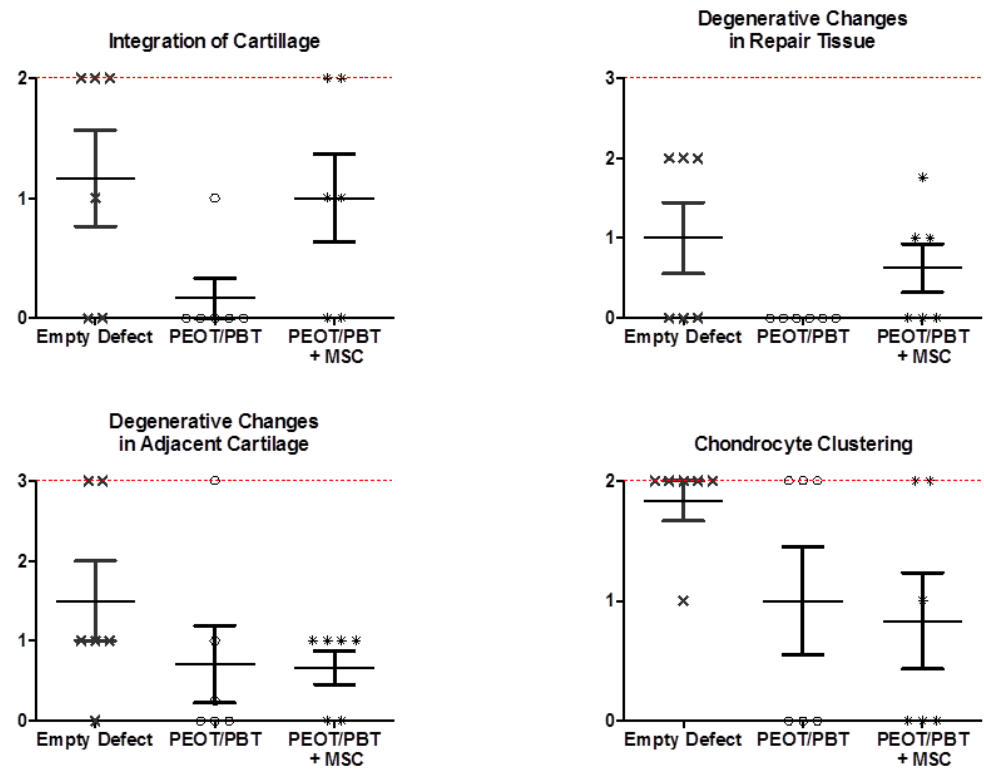


Figure 6A Histological scoring for hyaline cartilage repair



1  
2  
3  
4  
5  
6  
7  
8  
9  
10  
11  
12  
13  
14  
15  
16  
17  
18  
19  
20  
21  
22  
23  
24  
25  
26  
27  
28  
29  
30  
31  
32  
33  
34  
35  
36  
37  
38  
39  
40  
41  
42  
43  
44  
45  
46  
47  
48  
49  
50  
51  
52  
53  
54  
55  
56  
57  
58  
59  
60  
61  
62  
63  
64  
65

Figure 6B Histological scoring for integration with native cartilage and degeneration



Form for Disclosure of Potential Conflicts of Interest

[Click here to download Form for Disclosure of Potential Conflicts of Interest: coi\\_disclosure for annals of biomedical engineering\\_AN.pdf](#)

Form for Disclosure of Potential Conflicts of Interest

[Click here to download Form for Disclosure of Potential Conflicts of Interest: coi\\_disclosure for annals of biomedical engineering\\_FB.pdf](#)

Form for Disclosure of Potential Conflicts of Interest

[Click here to download Form for Disclosure of Potential Conflicts of Interest: coi\\_disclosure for annals of biomedical engineering\\_LM.pdf](#)

Form for Disclosure of Potential Conflicts of Interest

[Click here to download Form for Disclosure of Potential Conflicts of Interest: coi\\_disclosure for annals of biomedical engineering\\_MM.pdf](#)

Form for Disclosure of Potential Conflicts of Interest

[Click here to download Form for Disclosure of Potential Conflicts of Interest: coi\\_disclosure for annals of biomedical engineering\\_PH.pdf](#)

Form for Disclosure of Potential Conflicts of Interest

[Click here to download Form for Disclosure of Potential Conflicts of Interest: coi\\_disclosure VB.pdf](#)

Form for Disclosure of Potential Conflicts of Interest

[Click here to download Form for Disclosure of Potential Conflicts of Interest: coi\\_disclosure for annals of biomedical engineering\\_CvB.pdf](#)

Form for Disclosure of Potential Conflicts of Interest

[Click here to download Form for Disclosure of Potential Conflicts of Interest: CoI FINAL VERSION GOM.pdf](#)

Form for Disclosure of Potential Conflicts of Interest

[Click here to download Form for Disclosure of Potential Conflicts of Interest: coi\\_disclosure CMC.pdf](#)

Form for Disclosure of Potential Conflicts of Interest

[Click here to download Form for Disclosure of Potential Conflicts of Interest: coi\\_disclosure for annals of biomedical engineering.pdf\\_SA.p](#)

Form for Disclosure of Potential Conflicts of Interest

[Click here to download Form for Disclosure of Potential Conflicts of Interest: coi\\_disclosure EC.pdf](#)

Form for Disclosure of Potential Conflicts of Interest

[Click here to download Form for Disclosure of Potential Conflicts of Interest: coi\\_disclosure JH.pdf](#)

Form for Disclosure of Potential Conflicts of Interest

[Click here to download Form for Disclosure of Potential Conflicts of Interest: coi\\_disclosure for annals of biomedical engineering KM.pdf](#)

Form for Disclosure of Potential Conflicts of Interest

[Click here to download Form for Disclosure of Potential Conflicts of Interest: coi\\_disclosure AM.pdf](#)

Form for Disclosure of Potential Conflicts of Interest

[Click here to download Form for Disclosure of Potential Conflicts of Interest: coi\\_disclosure FS.pdf](#)

Form for Disclosure of Potential Conflicts of Interest

[Click here to download Form for Disclosure of Potential Conflicts of Interest: coi\\_disclosure GS.pdf](#)